A multi-stimuli responsive gold nanocage-hyaluronic platform for targeted photothermal and chemotherapy

ARTICLE *in* BIOMATERIALS · AUGUST 2014

Impact Factor: 8.56 · DOI: 10.1016/j.biomaterials.2014.08.013 · Source: PubMed

8 AUTHORS, INCLUDING:

Zhenzhen Wang
Chinese Academy of Sciences
9 PUBLICATIONS **19** CITATIONS
SEE PROFILE

Zhaowei Chen
Chinese Academy of Sciences
25 PUBLICATIONS **235** CITATIONS
SEE PROFILE

Zhen Liu
140 PUBLICATIONS **727** CITATIONS
SEE PROFILE

Biomaterials xxx (2014) 1–11

Contents lists available at ScienceDirect

Biomaterials

journal homepage: www.elsevier.com/locate/biomaterials

A multi-stimuli responsive gold nanocage–hyaluronic platform for targeted photothermal and chemotherapy

Zhenzhen Wang [a, b], Zhaowei Chen [a, b], Zhen Liu [a], Peng Shi [a, b], Kai Dong [a, b], Enguo Ju [a, b], Jinsong Ren [a, *], Xiaogang Qu [a, *]

[a] State Key Laboratory of Rare Earth Resources Utilization and Laboratory of Chemical Biology, Changchun Institute of Applied Chemistry, Chinese Academy of Sciences, Changchun 130022, PR China
[b] Graduate School of University of Chinese Academy of Sciences, Beijing 100039, PR China

ARTICLE INFO

Article history:
Received 30 June 2014
Accepted 8 August 2014
Available online xxx

Keywords:
Gold nanocages
Hyaluronic acid
Multi-stimuli responsive
Intracellular drug delivery
Synergistic therapy

ABSTRACT

Noninvasive and pinpointed intracellular drug release that responds to multiple stimulus is still a formidable challenge for cancer therapy. Herein, we reported a multi-stimuli responsive platform based on drug loaded gold nanocages @ hyaluronic acid (AuNCs-HA) for pinpointed intracellular drug release. These well-prepared nanohybrids could specifically recognize cancer cells via HA-CD44 interactions and be efficiently endocytosed by receptor-mediated process. Subsequently, the coated HA molecules could be degraded in lysosomes, resulting in the release of encapsulated drug. In addition, by taking advantage of the excellent photothermal properties, the AuNCs could accelerate the release of encapsulated drug and induce a higher therapeutic efficacy upon near-infrared (NIR) irradiation. In vitro results confirmed that the encapsulated drug could only be pinpointedly released in intracellular environments, which permitted high therapeutic efficacy against cancer cells and minimized the side effects. Importantly, as compared to that of the two therapies independently, a complete inhibition of tumor growth treated with the combination of chemotherapy and photothermal therapy was observed in vivo. Taken together, our present study provides new insights into developing pinpointed, multi-stimuli responsive intracellular drug release systems for synergistic cancer therapy.

1. Introduction

Recently, owing to their site-selective and controlled-release pattern, enhanced therapeutic efficacy and reduced side effect, stimuli-responsive drug delivery systems have attracted much attention [1–3]. Importantly, these admirable systems could minimize premature drug release in the circulating blood pool, maximize tumor-directed drug delivery efficiency, as well as offer obvious merits of precision spatial, temporal and dose control via a remote apparatus [4–7]. To date, various stimuli-responsive drug delivery systems have been reported, including pH, temperature [8], enzyme [9], photoirradiation, redox [2], competitive binding, electrical stimuli [10] and host-guest interactions. Especially, the integration of multiple stimulus could provide a unique opportunity to further fine-tune their response to each stimulus, as well as precisely regulate release profile. For example, Huang and co-workers have recently reported a multifunctional nanoplatform based on mesoporous silica-coated graphene nanosheets that showed heat-stimulative, pH-responsive, and sustained release properties [11]. In addition, Liu et al. have reported nano-supramolecular binary vesicles based on host-guest complexation that responded to external stimuli, including temperature, host-guest inclusion, and redox [2]. Although promising, all these systems are compromised by releasing drugs in tumor extracellular environment upon multi stimuli, or/and being incapable of completely eliminating premature drug release before being internalized. Meanwhile, some of the nanoparticles were found to localize on the cell membrane or remain in the intercellular medium of tumor cells, where the encapsulated drug could also be released upon external stimuli [12–14]. Owing to rapid excretion into the blood stream, these unexpected released drugs would bring side effects to adjacent normal tissues and even the evocation of the multi-drug resistance [10,15–19]. Therefore, the development of pinpointed intracellular drug release system that responds to multi stimuli is highly desired in cancer treatment.

Recently, with hollow interiors, porous walls and tunable localized surface plasmon resonance peaks (LSPR) in the NIR region, gold nanocages have become a new promising platform for

* Corresponding authors. Tel/fax: +86 0431 85262625.
E-mail addresses: jren@ciac.ac.cn (J. Ren), xqu@ciac.ac.cn (X. Qu).

http://dx.doi.org/10.1016/j.biomaterials.2014.08.013
0142-9612/

therapeutic applications [20,21]. For example, upon exposure to a NIR laser beam with a wavelength that matches the absorption peak of the AuNCs, light will be absorbed and converted into heat with high efficacy [22,23]. Subsequently, the heat will dissipate into the surroundings and stimulate the drug release [24–26]. Thus, the unique structures of AuNCs make them well suited for drug encapsulation and photothermal controlled drug release with high spatial and temporal resolution. However, their practical applications are limited by the following drawbacks: 1) Without any surface modification, AuNCs were unstable under physiological conditions, which is not suitable for in vivo drug delivery [27]; 2) These AuNCs-based system might suffer from premature drug leakage due to their intrinsic hollow interiors and pores; 3) Extracellular drug leakage still exists upon multi stimuli by using AuNCs as nanocarriers alone. Therefore, how to make it to realize pinpointed intracellular drug release in response to multi stimuli remains a big challenge in this field. As one of the extracellular matrix components, HA is a negatively charged, naturally occurring polysaccharide with nonimmunogenic, non-toxic and biodegradable characters [28–31]. Intriguingly, HA has been used as a drug carrier or targeting moiety due to the specific interaction with CD44, which is overexpressed on various cancer cells [32–35]. Furthermore, HA could be specially degraded into low molecular weight fragments by intracellular lysosomal enzyme hyaluronidase (Hyal). As a result, HA could be utilized as targeting and capping agent for cell-specific targeted and controlled drug release in response to Hyal presented at intracellular microenvironments [36–40]. Therefore, we envision that the integration of the intracellular enzyme responsive property of HA and the unique advantages of AuNCs would provide the potential for multi-stimuli responsive and pinpointed intracellular drug release.

Herein, we designed a multi-stimuli responsive nanoplatform based on drug loaded AuNCs@HA for pinpointed intracellular drug release and targeted synergistic therapy. Different from previously reported multi-stimuli responsive platform, the key concept of our delivery system lies on the pH and NIR stimuli can be activated to trigger the release of encapsulated drug only after nanoparticles were internalized (Scheme 1). This advantage could be anticipated to confer our system the pinpointed intracellular drug release ability upon exposing to multiple stimulus. Meanwhile, the tumor-targeting ability should be realized because of the interactions between HA and CD44. According to our design, another exciting feature is that the excellent synergistic effect of combining chemotherapy and photothermal therapy. And the unexceptionable synergistic therapy was be explored by the ablation of tumor both in vitro and in vivo. We believe that the rational integration of these functionalities would remarkably enhance the therapeutic efficiency while minimizing side effects.

2. Materials and methods

2.1. Materials

N-hydroxysulfosucnimide sodium salt (sulfo-NHS) was purchased from Pierce Biotechnology. 1-[3-(dimethylamino) propyl]-3-ethylcarbodiimide hydrochloride (EDC) was obtained from Alfa Aesar. Doxorubicin (Dox), $AgNO_3$ (more than 99%), poly (vinyl pyrrolidone) (PVP, average Mr E 29,000 or 55,000) and $HAuCl_4{-}3H_2O$ (99.9+%) were all purchased from Sigma Aldrich (Boston, MA, USA). Dopamine hydrochloride (DA) and Sodium hyaluronate (MW ≈ 100 KDa) were purchased from Aladdin. Hyaluronidase from bovine vitreous humor was Shanghai Sangon Biological Engineering Technology & Services. All chemicals were used as received from the suppliers without further purification. Ultrapure water (18.2 MΩ; Millpore Co., USA) was used throughout the experiment.

2.2. Measurements and characterizations

FITR analyze was carried out on a Bruker Vertex 70 FITR Spectrometer. Scanning transmission electron microscopy (SEM) images were obtained with a Hitachi S-4800 FE-SEM. Ultraviolet–visible (UV–Vis) spectroscopy spectra were recorded with a JASCO-V550 spectrometer. Transmission electron microscopy (TEM) images were recorded using a FEI TECNAI G2 20 high-resolution transmission electron microscope operating at 200 kV. The zeta potential of the nanoparticles in water was measured in a Zetasizer 3000HS analyser. Dynamic Light Scatterer (DLS) was made by Malvern Corp, UK (ZEN3690). Fluorescence spectra were recorded with a JASCO

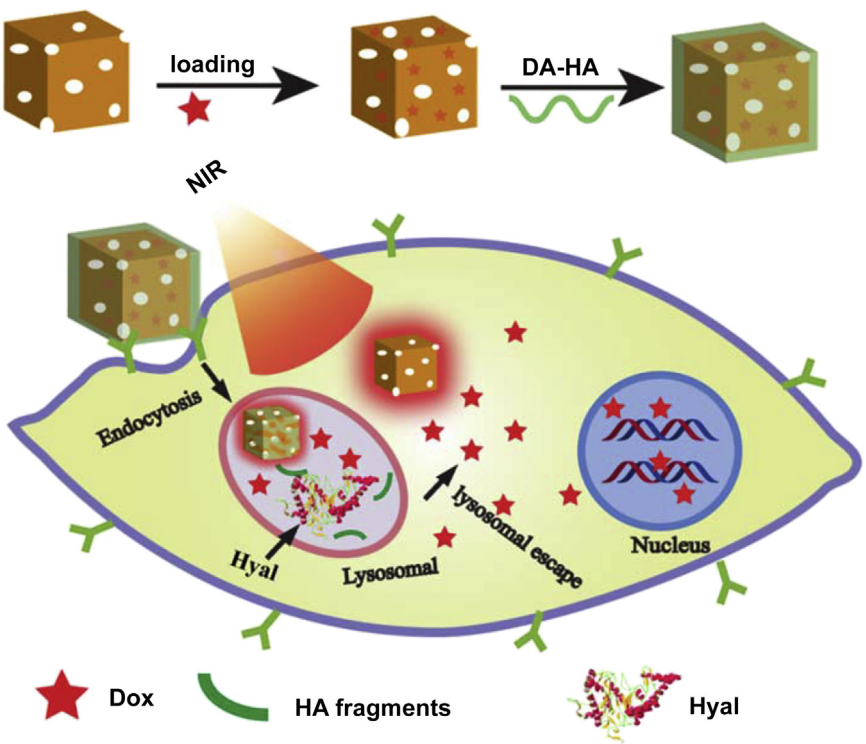

Scheme 1. Schematic representation of a multi-stimuli responsive platform based on Dox loaded AuNCs-HA nanoparticles for pinpointed intracellular drug release and synergistic therapy.

Please cite this article in press as: Wang Z, et al., A multi-stimuli responsive gold nanocage–hyaluronic platform for targeted photothermal and chemotherapy, Biomaterials (2014), http://dx.doi.org/10.1016/j.biomaterials.2014.08.013

FP-6500 spectrofluorometer. A CWdiode laser (LSR808NL-2000) with wavelength of 808 nm was used for the laser irradiation experiment.

2.3. Synthesis of gold nanocages

AuNCs were synthesized according to a previously reported method. Briefly, poly (vinyl pyrrolidone) (PVP, 1 mg/mL) was added to 5 mL of deionized water to form homogenous solution and then 500 μL of the Ag nanocubes (3 nM) was added the solution. The above solution was heated to boil for 10 min. Subsequently, The $HAuCl_4$ (0.5 mM) was added to the flask at a rate of 45 mL/h. The solution was refluxed for another 30 min until the color of the reaction was stable. Once cooled to room temperature, the sample was centrifuged and washed with saturated NaCl solution to remove AgCl and with water several times to remove PVP and NaCl.

2.4. Synthesis of HA-DA

HA (0.1 g) was dissolved in degassed 50 mL of phosphate buffered saline (PBS) buffer. EDC (50 mg) and NHS (30 mg) were added to the mixed solution, until the final molar ratio of HA/EDC/NHS was set to 1:1:1. Then, 50 mg of DA was added to the above mixture. The pH value of the solution was continuously monitored and maintained from 4 to 6 for 9 h. After the reaction, the solution was purified by dialysis (MWCO = 14000) for 2 day in PBS (20 mM, pH 7.4) and was subsequently lyophilized, which resulted in a white powder.

2.5. Dox loading and HA-DA capping

Dox was first loaded inside AuNCs as follows: AuNCs was incubated in the PBS (10 mM, pH 7.4) of Dox (0.2 mM) for 24 h under stirring at room temperature, followed by centrifuging and washing with PBS buffer (10 mM, pH 7.4) to remove any residual free Dox. Then, HA-DA was added to the suspension, and the mixture was stirred for another 24 h, followed by centrifuging and repeated washing with PBS buffer (10 mM, pH 7.4). All the washing solutions were collected, and the loading of Dox was calculated from the difference in the concentration of the initial and left Dox.

2.6. Synthesis of GFP-AuNCs-HA

Green fluorescent protein (GFP) exhibits intense green fluorescence under UV light. This property allows the use of fluorescence to study the distribution of AuNCs-HA nanoparticles inside the cells. GFP labeled AuNCs-HA nanoparticles were synthesized as follows: EDC (10 mg) and NHS (10 mg) were dissolved in 5 mL of MES buffer (pH 6.0) in the presence of AuNCs (5 mg). The mixed solution was stirred for 3 h. Then, GFP was added and then the mixture was stirred for another 12 h. After that, the solution was centrifuged and washed to remove any residual free GFP.

2.7. Multi-stimuli responsive release experiments

To investigate the action of NIR and Hyal for Dox released at different pH values, the Dox-AuNCs-HA nanoparticles were dispersed in the aqueous buffer solutions (pH 7.4 of PBS buffer, pH 5.5 and 4.5 of acetate buffer) with or without Hyal (150 U/ml) at 37 °C. Aliquots (50 μL) were taken from the suspension at pre-determined time intervals, and replaced with an equal volume of the fresh medium, the released samples were centrifuged. The concentration of released Dox was determined by measurement of UV–Vis spectra at 480 nm based on the standard curve.

2.8. Cell culture

MDA-MB-231 and NIH-3T3 cells were cultured in 25 cm^2 flasks in Isceve's Modified Dulbecco's medium (IMDM) (Gibco) containing 10% (v/v) fetal bovine serum (Gibco) at 37°C in an atmosphere of 5% (v/v) CO_2 in air. The media were changed every two days, and the cells were passaged by trypsinization before confluence.

2.9. Confocal laser scanning microscopy (CLSM)

A suspension of GFP labeled AuNCs-HA nanoparticles in PBS was introduced to culture medium overnight to mimic the blood circulation process prior to the cellular uptake. MDA-MB-231 and NIH3T3 cells were then incubated with nanoparticles in medium for 2 h, and then after washing free nanoparticles, 10 μM lysotracker was added for staining of the lysosomes of cancer cells for further 0.5 h incubation. Finally, the cells were washed three times with PBS and transferred to serum free medium and then examined by CLSM.

2.10. Fluorescene imaging

MDA-MB-231 cells were seeded in a 24-well plate and cultured for 24 h. The cell medium was removed, and then cells were incubated with 0.5 mL of fresh cell medium containing 25 μg of Dox-AuNCs-HA for 2 h. After that, the medium was replaced by fresh cell medium to remove free nanoparticles. And then MDA-MB-231 cells were incubated for another 1 h and 10 h. At last, the medium was replaced by cell medium with Hoechst. Cell imaging was then carried out after washing cells with PBS.

2.11. In vitro cytotoxicity assays

Methyl thiazolyl tetrazolium (MTT) assays were used to probe cellular viability. MDA-MB-231 cells were seeded at a density of 5000 cells/well in 96-well assay plates. Drugs at the indicated concentrations were added and cells were further incubated for 24 h to allow the uptake of nanoparticles. To determine toxicity, 10 μL of MTT solution (BBI) was added to each well of the microtiter plate and the plate was incubated in the CO_2 incubator for an additional 4 h. The cells then were lysed by the addition of 100 μL of DMSO. Absorbance values of formazan were determined with Bio-Rad model-680 microplate reader at 490 nm (corrected for background absorbance at 630 nm). The excellent synergistic effect of the combination of photothermal therapy and chemotherapy was estimated using the relation of $P_{additive} = (f_1 \times f_2) \times P_0$, where $P_{additive}$ is the final population after an additive interaction, P_0 is the initial population and f_1 is the fraction of surviving cells after chemotherapy treatment, f_2 refers the photothermal therapy [41]. The results were expressed as the mean values of three measurements.

2.12. Biodistribution assays of AuNCs-HA

For biodistribution study, six MDA-MB-231 tumor-bearing mice (tumor size ≈ 200 mm^3) were randomly put into two groups. One group was intravenously injected with AuNCs (1 mL, 1 mg/mL) via the tail vein and the gold concentration in AuNCs nanoparticles solution was 0.71 mg/mL. The other was intravenously injected with AuNCs-HA (1 mL, 1 mg/mL) and the gold concentration was 0.39 mg/mL. After 24 h, the organs (heart, liver, spleen, lung, kidneys and tumors) were surgically removed. The Au ions were quantified through ICP-MS method. The organs were placed into a flask containing 4 mL of aqua regia, and incubated for 8 h under heat treatment (80 °C) for dissolution of the tissues. The obtained liquid was subjected to ICP-MS analysis. The Au content % was analyzed by using the concentration of gold in organ divided by the concentration of gold in nanoparticle solution respectively.

2.13. Antitumor activity in vivo

The MDA-MB-231 cells were inoculated into the nude mice. When the tumor size reached about 200 mm^3, mice were divided into four groups consisting of 5 mice in each group. After that, group 1 and 3 were injected intratumorally with 0.9% NaCl (50 μL) and 0.1 mg/mL Dox-AuNCs-HA (50 μL) respectively. Mice in group 2 and 4 received intratumorally the injections of 0.1 mg/mL (50 μL) AuNCs-HA and 0.1 mg/mL Dox-AuNCs-HA (50 μL), and were followed by NIR irradiation (1 W/cm^2, 5 min) after each drug injection. Then the tumor size dimensions were measured with a caliper every day, and the tumor volume was calculated according to the equation: Volume = (Tumor Length) × (Tumor Width)^2/2. All animal procedures were in accord with the guidelines of the Institutional Animal Care and Use Committee.

2.14. Statistical analysis

All data were expressed in this article as mean result ± standard deviation (SD). All figures shown in this article were obtained from several independent experiments with similar results. Statistical evaluation was performed using analysis of variance (Student's *t*-test). A *p*-value <0.05 was considered statistically significant.

3. Results and discussion

We carried out a series of experiments to demonstrate our above design. Firstly, AuNCs were synthesized as previously reported and characterized by the TEM and SEM [42]. As depicted in Figure S1 and Fig. 1A, the size of AuNCs was about 50 nm and the pore size was about 5–8 nm. Moreover, the as-prepared AuNCs were well dispersed and showed good uniformity. By changing Au/Ag alloy aspect ratio, the LSPR peak of the obtained AuNCs was tuned to about 796 nm to match the central wavelength of the NIR irradiation source (Fig. 1C). Next, in order to prevent the premature release of drugs, HA-dopamine (HA-DA) was synthesized to conjugate on the surface of AuNCs via strong Au-catechol bonds (Figure S2). The extent of DA conjugation in the HA was determined by UV–Vis spectroscopy at 280 nm using DA standard solutions, with results showing that approximately 10% of the carboxylic acid groups in the HA chain were conjugated with DA. As shown in Fig. 1D, the single absorbance peak appeared at 280 nm, and the absence of additional peaks at wavelengths longer than 300 nm indicated that the conjugated DA was not oxidized [28]. Subsequently, the successful grafting of HA onto the surface of AuNCs was validated by various methods. TEM images provided direct evidence of the HA distribution on the surface of AuNCs due to an obvious coating morphology (Fig. 1B). In addition, the strong

Please cite this article in press as: Wang Z, et al., A multi-stimuli responsive gold nanocage–hyaluronic platform for targeted photothermal and chemotherapy, Biomaterials (2014), http://dx.doi.org/10.1016/j.biomaterials.2014.08.013

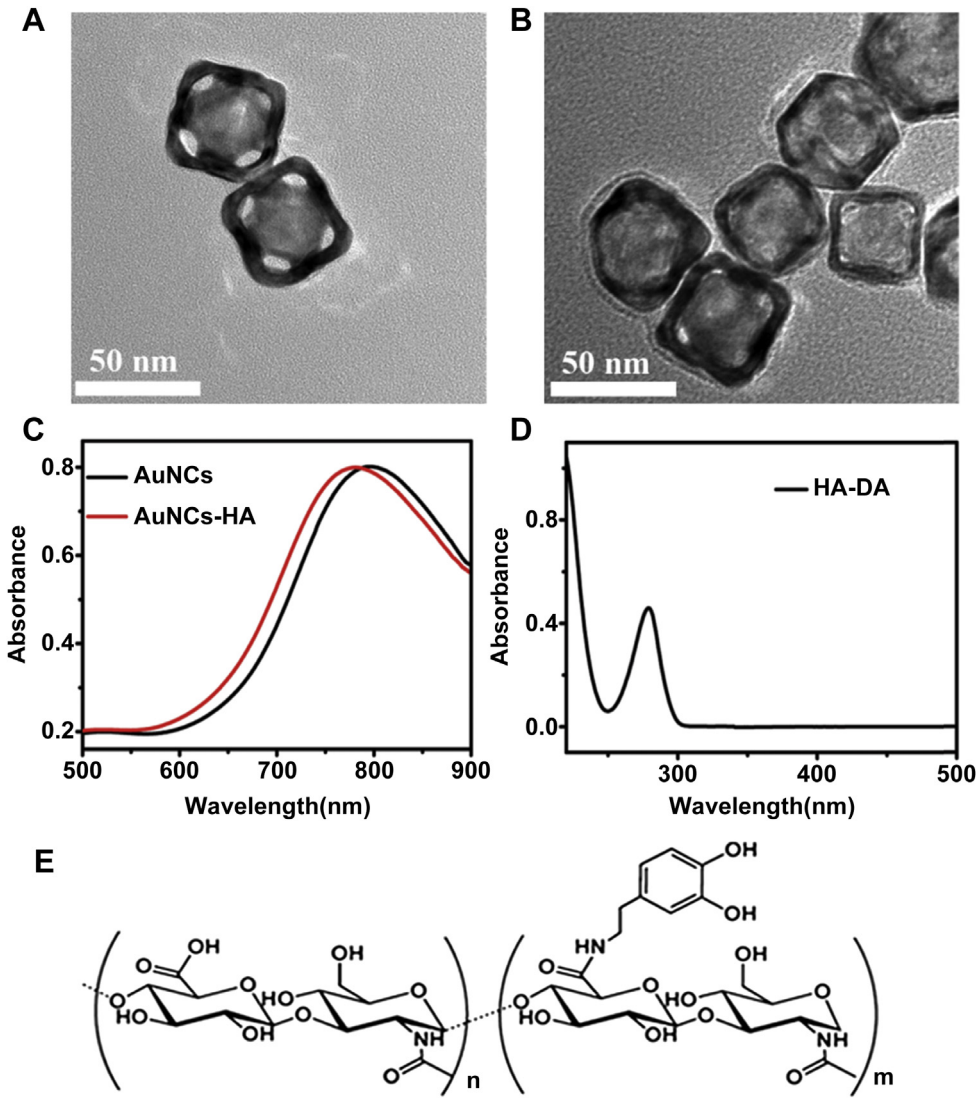

Fig. 1. A) TEM micrograph of AuNCs. B) TEM micrograph of HA capped AuNCs. C) UV–Vis absorption spectra of AuNCs and AuNCs-HA. D) UV–Vis absorption spectra of HA-DA. E) The molecular structure of HA-DA.

–CO–NH- bending at 1520 cm^{-1} and 1660 cm^{-1} in FT-IR spectrum also indicated that the HA was grafted on the surface of AuNCs successfully (Figure S3). Compared with AuNCs, the LSPR peak of AuNCs-HA at 780 nm further supported the successful synthesis of AuNCs-HA and the little blue shifted emission peak might attribute to the excellent dispersion of the nanoparticles (Fig. 1C). Additionally, to obtain more insight into the nanoparticles, the surface charge was examined using zeta potential measurement in distilled water. The corresponding zeta potential of the AuNCs was −6.52 ± 2.82 mV, however, the zeta potential of AuNCs-HA was −25.76 ± 2.91 mV (Table S1). Typically, strongly negative zeta-potential enables individual dispersion of nanoparticles [16]. Indeed, we observed that AuNCs-HA was stable in buffer solution over a long period without any precipitation, which was further demonstrated by the no significant variation of hydrodynamic diameter of AuNCs-HA (Figure S4). Taken together, the size and the charge of AuNCs-HA were suitable for systemic cancer therapy and could provide additional advantages for longer blood circulation and effective tumor accumulation.

Previous studies have shown that AuNCs can be used as photothermal agents due to their tunable LSPR peaks in NIR region [21]. To demonstrate the potential of AuNCs for photothermal cancer therapy, we exposed AuNCs (50 μg/ml) to NIR laser irradiation at 808 nm with a power density of 1 W cm^{-2} for 10 min. Changes in temperature were measured and imaged by a thermal camera over the duration of experiments. As shown in Fig. 2, the temperature of AuNCs aqueous solution increased by 22 °C in our experiment. In stark contrast, under the same conditions, the temperature of nanoparticle-free distilled water only increased by 2 °C. The superior photothermal efficiency of AuNCs not only provided potential for thermal ablation of malignant tissues [22], but also could accelerate desorption and release of the encapsulated drugs by the photothermal conversion of AuNCs [25]. In addition, AuNCs-HA exhibited great intracellular enzyme responsive property. As shown in Fig. 3A, the hydrodynamic diameter of the AuNCs-HA in the acetate buffer (pH 4.5) was 90 nm, however, the apparent hydrodynamic diameter decreased to 65 nm in the presence of Hyal. The corresponding zeta potential of the AuNCs-HA increased significantly in the presence of Hyal (Fig. 3B). This could be attributed to the fragmentation and detachment of the negatively charged HA on the surfaces. Furthermore, the polyacrylamide gel electrophoresis (PAGE) with Alcian Blue (in web version) and silver

Please cite this article in press as: Wang Z, et al., A multi-stimuli responsive gold nanocage–hyaluronic platform for targeted photothermal and chemotherapy, Biomaterials (2014), http://dx.doi.org/10.1016/j.biomaterials.2014.08.013

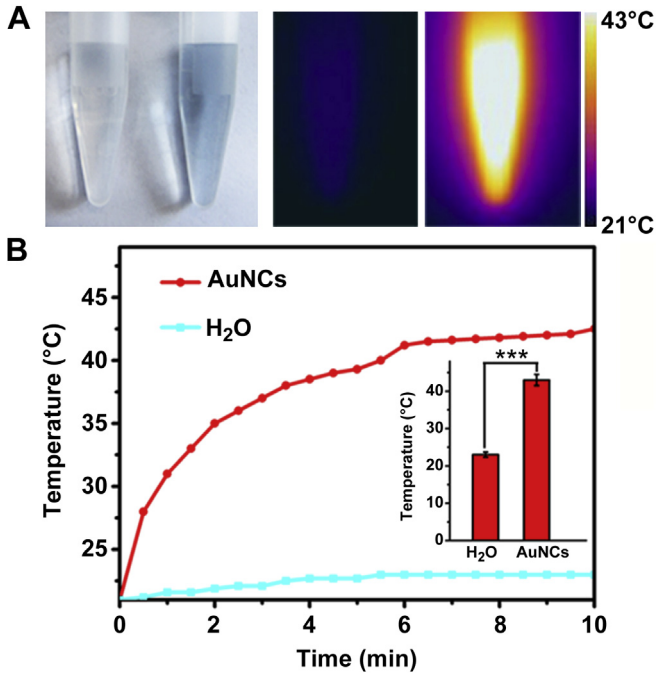

Fig. 2. Photothermal heating of AuNCs suspensions. A) Thermal images of AuNCs solution and distilled water after 10 min of 808 nm laser irradiation at 1 W. The AuNCs sample show significant photothermal heating, while the distilled water is not heated by the laser. B) Temperature measurements from thermal images acquired during the laser irradiation. The inset was final temperature of AuNCs solution and distilled water after 10 min of 808 nm laser irradiation at 1 W. The error is the standard deviation from the mean ($n = 5$). Asterisks indicate statistically significant differences ($^{*}P < 0.05$, $^{**}P < 0.01$, $^{***}P < 0.001$).

staining was also used to analysis the Hyal responsive property of AuNCs-HA [43]. As shown in Fig. 3C, Hyal resulted in obvious polymer fragmentation in the acetate buffer (pH 4.5) relative to the control groups. These results indicated that the intracellular enzyme Hyal could degrade HA into fragments with low molecular weight, which would be helpful for the uncapping of drug loaded AuNCs-HA and subsequent releasing of the encapsulated drugs.

To further confirm that intracellular enzyme and NIR could trigger and accelerate the release of drug, we performed related experiments as a function of different incubation periods upon various conditions. In our study, Dox, an effective and widely used chemotherapeutic agent [44], was selected as a modal anticancer agent. The amount of encapsulated Dox in the Dox-AuNCs-HA nanocomplex was quantitated to be 48 μg Dox/mg AuNCs-HA (Figure S5). As illustrated in Fig. 4A, only negligible Dox was released from Dox-AuNCs-HA in PBS buffer (pH 7.4) within 12 h. Moreover, no insignificant increase was observed under NIR laser irradiation (1 W, 808 nm). Meanwhile, we also observed similar release profiles of Dox at different pH values (Fig. 4B,C). These results suggested a good end-capping efficiency and stability of Dox-AuNCs-HA under simulated physiological conditions (pH 7.4) and intercellular medium of tumor cells (pH 5.5) even upon NIR irradiation. Next, we examined the drug release from the nanocomposites in the presence of Hyal at pH 4.5. Compared to the above results, a significant burst release of Dox was detected, which demonstrated the enzymatic degradation of coated HA and a stimuli-responsive opening process. In addition, a significantly enhanced release of Dox was determined upon NIR laser irradiation (Fig. 4C). The enhanced release of Dox upon NIR irradiation was ascribed to the remote heating generating by AuNCs through photothermal conversion, where the heating of the surrounding fluid decreases its viscosity and favors the diffusion of the drug away from the AuNCs [45]. All above results showed that without intracellular enzyme Hyal, neither pH nor NIR could trigger the release of Dox. In other words, only after the nanoparticles being internalized, the encapsulated drugs can be released upon the degradation of HA by intracellular Hyal, meanwhile the acidic pH and NIR stimuli would be effective to facilitate the release of Dox. Reasonably, our system could be anticipated to prevent any premature leakage upon external stimuli and enable the pinpointed intracellular drug release, which would dramatically improve the therapeutic efficacy and reduce adverse side effects of drugs.

We next extended the controlled release to a study for targeted drug delivery in vitro. Targeted delivery to specific cells is entailed in cancer therapy [26]. We first confirmed the cellular targeting efficiency by incubating NIH3T3 (control cells) and MDA-MB-231 (CD44 overexpressed) cell lines with GFP labeled AuNCs-HA. As illustrated in Fig. 5A, flow cytometry demonstrated that a large shift was observed for MDA-MB-231 cells treated with the GFP labeled AuNCs-HA, however, no significant shift was observed for NIH3T3 cells. The data clearly indicated that the GFP-AuNCs-HA nanoparticles could bind to and be internalized by MDA-MB-231 cells with high selectivity while showed little affinity to nontarget cells. The targeting specificity of GFP-AuNCs-HA were also confirmed by CLSM, as shown in Fig. 5B-b,f, MDA-MB-231 cells incubated with the GFP-AuNCs-HA nanoparticles showed strong fluorescence within the cells, whereas the GFP-AuNCs-HA nanoparticles exhibited much less binding and internalization ability when incubated with NIH3T3 cells. Moreover, when we used 5 mg/ml

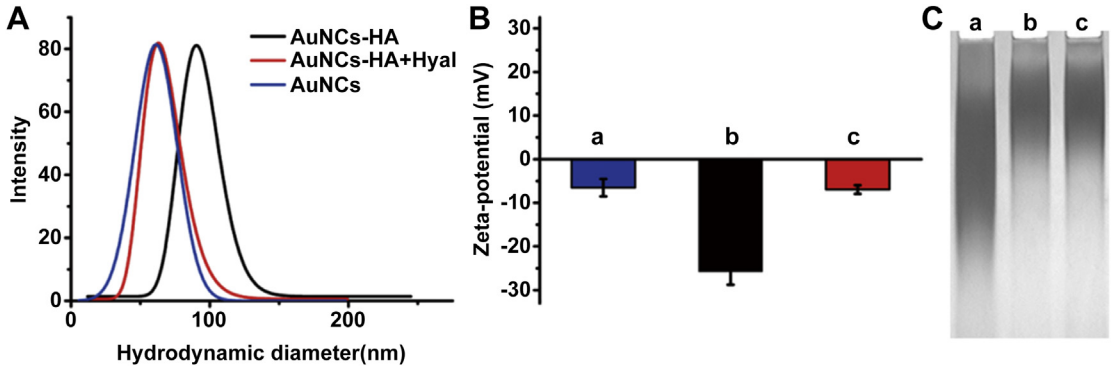

Fig. 3. The intracellular Hyal responsive properties of AuNCs-HA. A) Hydrodynamic diameter of AuNCs, AuNCs-HA and AuNCs-HA in the presence of Hyal measured in water. B) The corresponding zeta potentials of nanoparticles: AuNCs (a), AuNCs-HA (b), AuNCs-HA in the presence of Hyal (c). The error is the standard deviation from the mean ($n = 5$). C) PAGE analysis of Hyal treated AuNCs-HA samples, lanes a–c: (a) AuNCs-HA + Hyal in the acetate buffer (pH 4.5), (b) AuNCs-HA in the acetate buffer (pH 4.5), (c) AuNCs-HA in the PBS buffer (pH 7.4).

Please cite this article in press as: Wang Z, et al., A multi-stimuli responsive gold nanocage–hyaluronic platform for targeted photothermal and chemotherapy, Biomaterials (2014), http://dx.doi.org/10.1016/j.biomaterials.2014.08.013

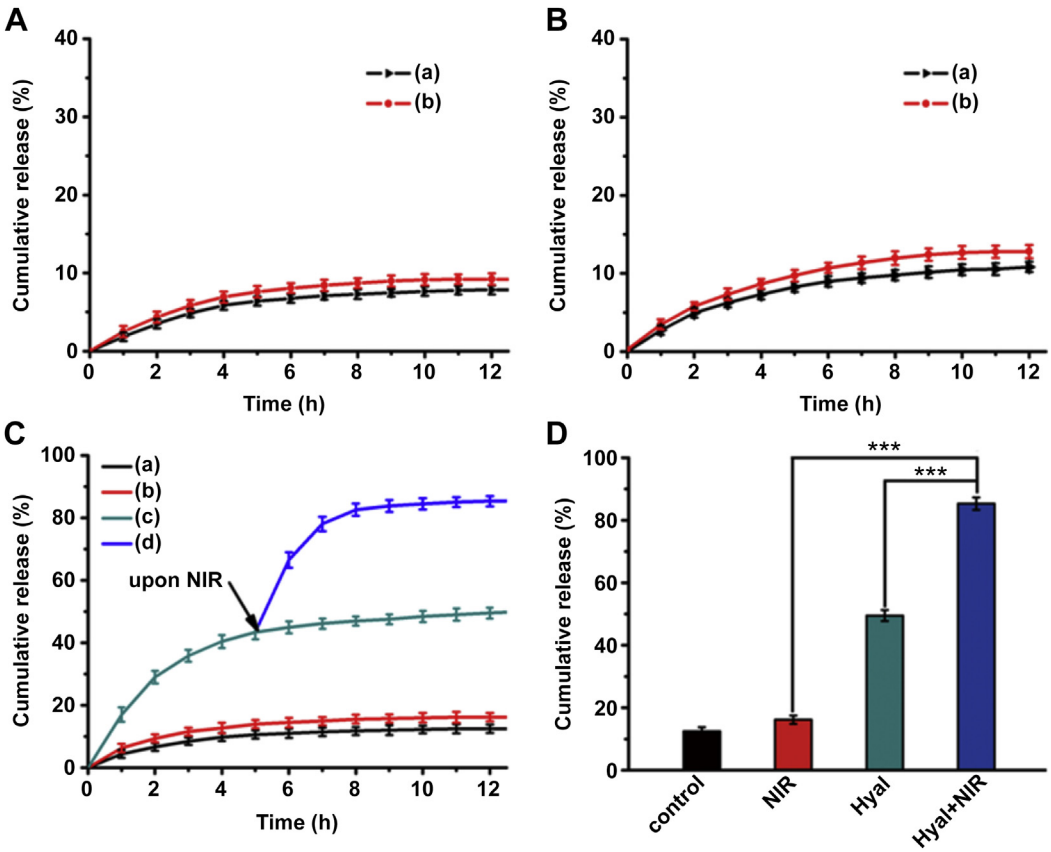

Fig. 4. A) B) Release profiles of Dox from Dox-AuNCs-HA nanoparticles in pH 7.4 PBS buffer and in pH 5.5 acetate buffer respectively: (a) control, (b) upon NIR irradiation. (C) The Dox release profiles from Dox-AuNCs-HA in acetate buffer at pH 4.5: (a) control, (b) upon NIR irradiation, (c) in the presence of Hyal, (d) in the presence of Hyal upon NIR irradiation. (D) The total cumulative release of Dox after 12 h. The error is the standard deviation from the mean ($n = 5$). Asterisks indicate significantly differences ($^{*}P < 0.05$, $^{**}P < 0.01$, $^{***}P < 0.001$).

free HA to incubate cells before cells treated with GFP-AuNCs-HA, a negligible shift was observed for both NIH3T3 cells and MDA-MB-231 cells (Fig. 5A). These results showed that the binding and uptake of GFP-AuNCs-HA into MDA-MB-231 cells could be prevented by excess HA due to the special interaction between HA and overexpressed CD44 on MDA-MB-231 cells. In addition, no binding occurred between NIH3T3 cells and the HA on the nanoparticles, neither shift nor enhancement was observed. Thus, the conjugation of HA on AuNCs successfully renders the system cancer cell target ability.

Previous studies have shown that HA nanocomposites were taken up into cells via receptor-mediated endocytosis and mainly resided in their acidic compartments such as endosomal and lysosomal vesicles [46]. Therefore, a co-localization study was carried out to determine whether AuNCs-HA accumulated within the lysosomes and endosomes after endocytosis. As shown in Fig. 5B, after 3 h of co-incubation with GFP-AuNCs-HA, green fluorescence of GFP appeared within MDA-MB-231 cells and co-localized with lysotracker red fluorescence, implying that the GFP-labeled nanoparticles were highly concentrated in the endosomes and lysosomes, which was in line with previous reported [46]. Therefore, we concluded that only after being endocytosed, the coated HA could readily degraded into lower molecular fragments by Hyal in subcellular components, which would allow pinpointed intracellular drug release upon exposing to multiple stimulus.

The success in controlling Dox release by multiple stimulus in vitro experiments promoted us to examine whether our delivery system could work in living cells. It is well known that gold nanomaterials is inert and could act as good quenchers of many fluorescence donors due to the nanosurface energy transfer effect [47,48]. As shown in Figure S6, the fluorescence of Dox loaded in AuNCs was quenched, while it recovered in the presence of intracellular enzyme Hyal. Thus, the intracellular fluorescence changes of Dox could be utilized to monitor the amount of released drugs. We next tested the detailed fluorescence intensity of Dox in MDA-MB-231 cells via co-incubation Dox-AuNCs-HA at 37°C (group 1) and 43°C (group 2). Dox-AuNCs-HA nanoparticles were incubated with cells for 2 h before washing the cells to remove unendocytosed nanoparticles and replacing with fresh medium. After further 1 h of incubation, only partial drug release with dim Dox fluorescence intensity was observed from group 1 (Fig. 6a). However, after exposure to NIR (0.5 h, 43°C), an obvious enhanced red fluorescence in the perinuclear cytoplasm and a slight Dox fluorescence within nuclei could be detected from group 2 (Fig. 6b). These results could be attributed to the fact that NIR stimuli could accelerate desorption and release of drugs from Dox-AuNCs-HA after the degradation of HA in acidic lysosomes [25]. Prolonging the incubation time to 12 h, bright red fluorescence could be observed in both cytoplasm and cell nuclei of MDA-MB-321 cells at 37°C (Fig. 6c). In contrast, much stronger fluorescence intensities could be detected in heated cells under NIR irradiation than that of cells incubated at 37 °C (Fig. 6d). Based on fluorescence microscopy images, we demonstrated that the combination of these multiple stimulus could result in more complete release of Dox. Meanwhile, AuNCs@HA was effective on holding Dox at unwanted extracellular

Please cite this article in press as: Wang Z, et al., A multi-stimuli responsive gold nanocage–hyaluronic platform for targeted photothermal and chemotherapy, Biomaterials (2014), http://dx.doi.org/10.1016/j.biomaterials.2014.08.013

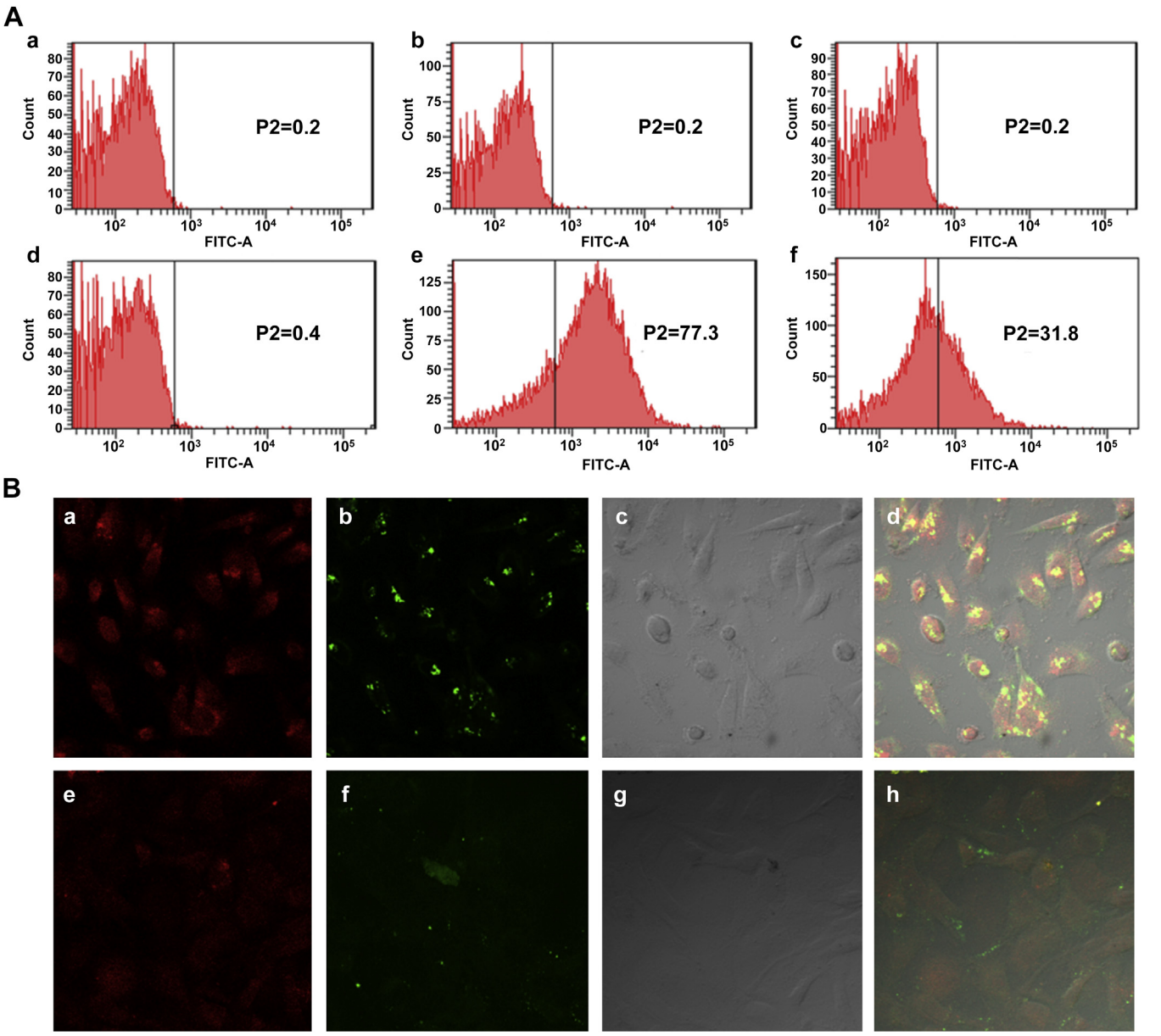

Fig. 5. A) Flow cytometry analysis to monitor the binding of GFP labeled AuNCs-HA nanoparticles with NIH3T3 (control cells a, b, c) and MDA-MB-231 cells (target cells d, e, f) respectively. (a), (d) cells only, (b), (e) GFP-AuNCs-HA, (c), (f) GFP-AuNCs-HA after preincubation for 2 h with free HA (5 mg/ml). B) CLSM investigation of the target ability and localization of GFP-AuNCs-HA to MDA-MB-231 cells (a, b, c, d) and NIH3T3 cells (e, f, g, h) each sample was imaged for (a), (e) lysotracker, (b), (f) GFP, (c), (g) bright field, and (d), (h) overlay. The images were obtained under magnification of 80.

compartments, which realized pinpointed intracellular drug release. Considering that the interaction of Dox with DNA is one of the major modes of action for Dox, thus, the release of Dox is crucial in playing its role in the growth inhibition of cancer cells [47].

To access the tumoricidal potential of our smart drug delivery system, cell viability was analyzed by MTT assay against MDA-MB-231 cells at various concentrations (5–50 μg/mL). Owing to the fact that AuNCs and HA all exhibit low- or non-cytotoxicity, AuNCs-HA showed a negligible effect on cancer cells even at a high concentration (Fig. 7A–a). In the following, the synergistically enhanced anticancer effect of the combined photothermal therapy and chemotherapy was quantified. We found that AuNCs-HA with NIR irradiation (photothermal therapy) or Dox-AuNCS-HA (chemotherapy) only induced a moderate growth inhibition of MDA-MB-231 cells (Fig. 7A-b, c). In stark contrast, when cells were incubated with Dox-AuNCs-HA upon NIR irradiation, the cell viability was remarkably reduced to 18% (Fig. 7A–e). Note that the efficacy of the combined treatment was significantly higher than those of the additive therapeutic efficacy of chemotherapy and photothermal treatments, indicating an excellent synergistic effect (Fig. 7B). The relatively low toxicity of Dox-AuNCs-HA in comparison to free Dox could attribute to gradual release of Dox within cells [49]. Furthermore, the cell viability was tested with LIVE (green)/DEAD (red) kit by fluorescent microscopy and confirmed that the cell viability was distinguishing following different treatments. As shown in Fig. 7C, a clear demarcation line between dead (red) and live cell (green) regions could be observed in the presence of AuNCs-HA upon NIR irradiation. By contrast, the nanoparticles themselves cannot lead to cell death, which implied that the AuNCs-HA was non-toxic. For cells treated with Dox-AuNCs-HA, the

Please cite this article in press as: Wang Z, et al., A multi-stimuli responsive gold nanocage–hyaluronic platform for targeted photothermal and chemotherapy, Biomaterials (2014), http://dx.doi.org/10.1016/j.biomaterials.2014.08.013

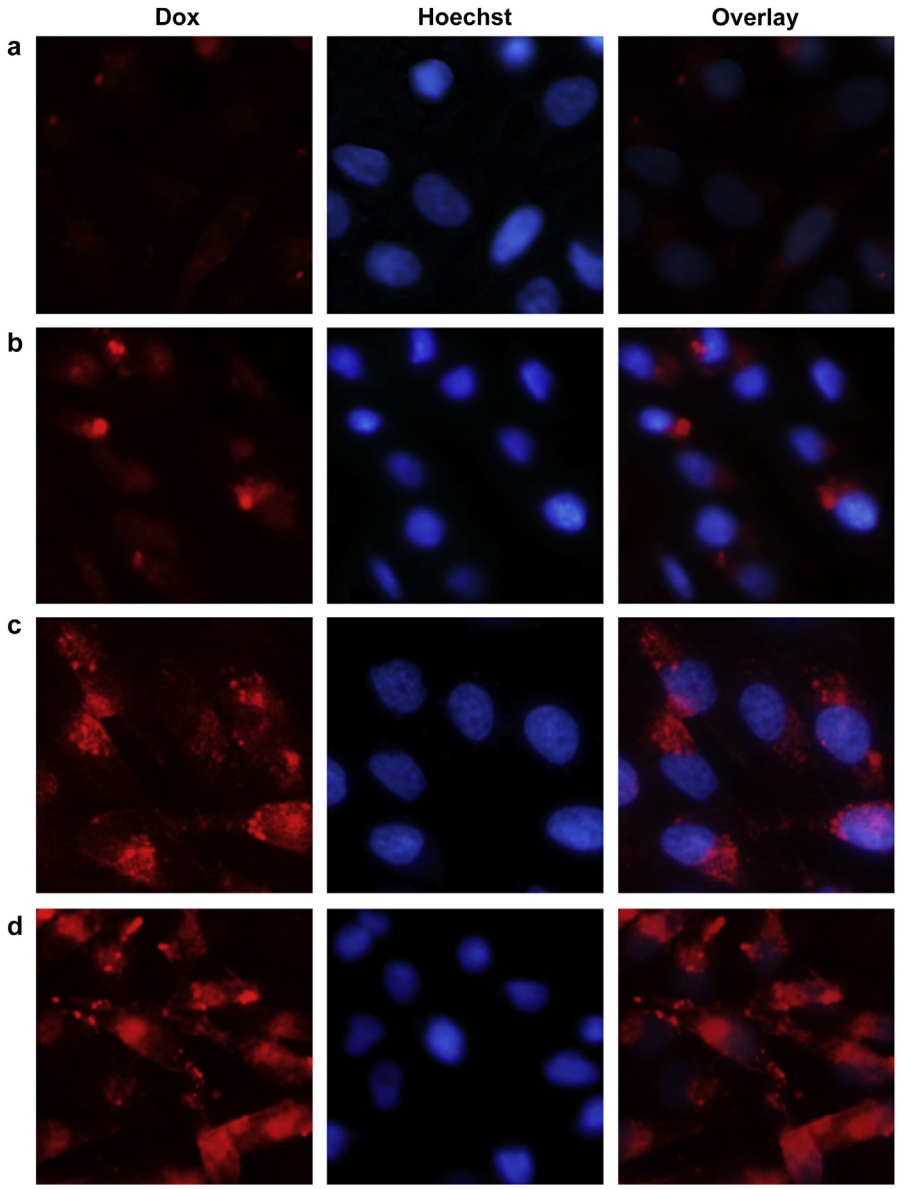

Fig. 6. Fluorescence microscopy images of MDA-MB-231 cells incubated with Dox-AuNCs-HA for 3 h (a), 12 h (c) at 37 °C or Dox-AuNCs-HA with NIR irradiation (0.5 h, 43 °C) for 3 h (b), 12 h (d). The dose of Dox was 1.45 μg/ml. Blue fluorescence is associated with Hoechst; the red fluorescence is expressed by released Dox. All images were obtained under magnification of 80.

viability was in line with MTT results. As expected, almost all cells were destroyed after being incubated with Dox-AuNCs-HA and exposed to the NIR laser at 1 W/cm^2 for 10 min (Fig. 7C–d). All these results clearly demonstrated that photothermal therapy combined with certain chemotherapeutic drugs could result in super additive or synergistic effect which was greater than the projected sum of these two treatments alone. Thus, our multi-stimuli responsive system could be an effective platform for inhibiting cancer cells growth by combining photothermal therapy and chemotherapy.

We next explored the death mechanism by flow cytometry experiments using annexin V-fluorescein isothiocyanate (Annexin V-FITC) and propidium iodide (PI) staining assay. Annexin V-FITC can identify apoptotic cells by binding to phosphatidylserine translocated from the inner to the outer leaflet of the cell membrane, whereas PI is impermeant to live cells and early apoptotic cells [19]. Corresponding with the MTT results, significantly higher proportion of cell population treated with the chemotherapy and photothermal therapy is Annexin V-FITC positive as compared to that of the two therapies independently (Fig. 7D). These results evidently substantiated that the Dox-AuNCs-HA with NIR irradiation could induce MDA-MB-231 cell apoptosis by a synergistic apoptosis-accelerating effect [50]. Compared to necrosis, apoptosis is a more benign form of controlled cell death without releasing of harmful cellular waste, which minimizes inflammation and damage to surrounding cells [50].

Finally, to assess the in vivo antitumor efficacy of our system, the MDA-MB-231 tumor-bearing nude mice model was employed. Firstly, we investigated the biodistribution of AuNCs and AuNCs-HA which were intravenously injected into nude mice. After the nanoparticles had circulated in the body of mice for 24 h, all of these nude mice were sacrificed and the concentration of Au in each organ was measured using ICP-MS. As illustrated in Fig. 8A, a relatively larger fraction of administered AuNCs-HA was preferentially accumulated Au amount in the tumor than that of AuNCs. It is

Please cite this article in press as: Wang Z, et al., A multi-stimuli responsive gold nanocage–hyaluronic platform for targeted photothermal and chemotherapy, Biomaterials (2014), http://dx.doi.org/10.1016/j.biomaterials.2014.08.013

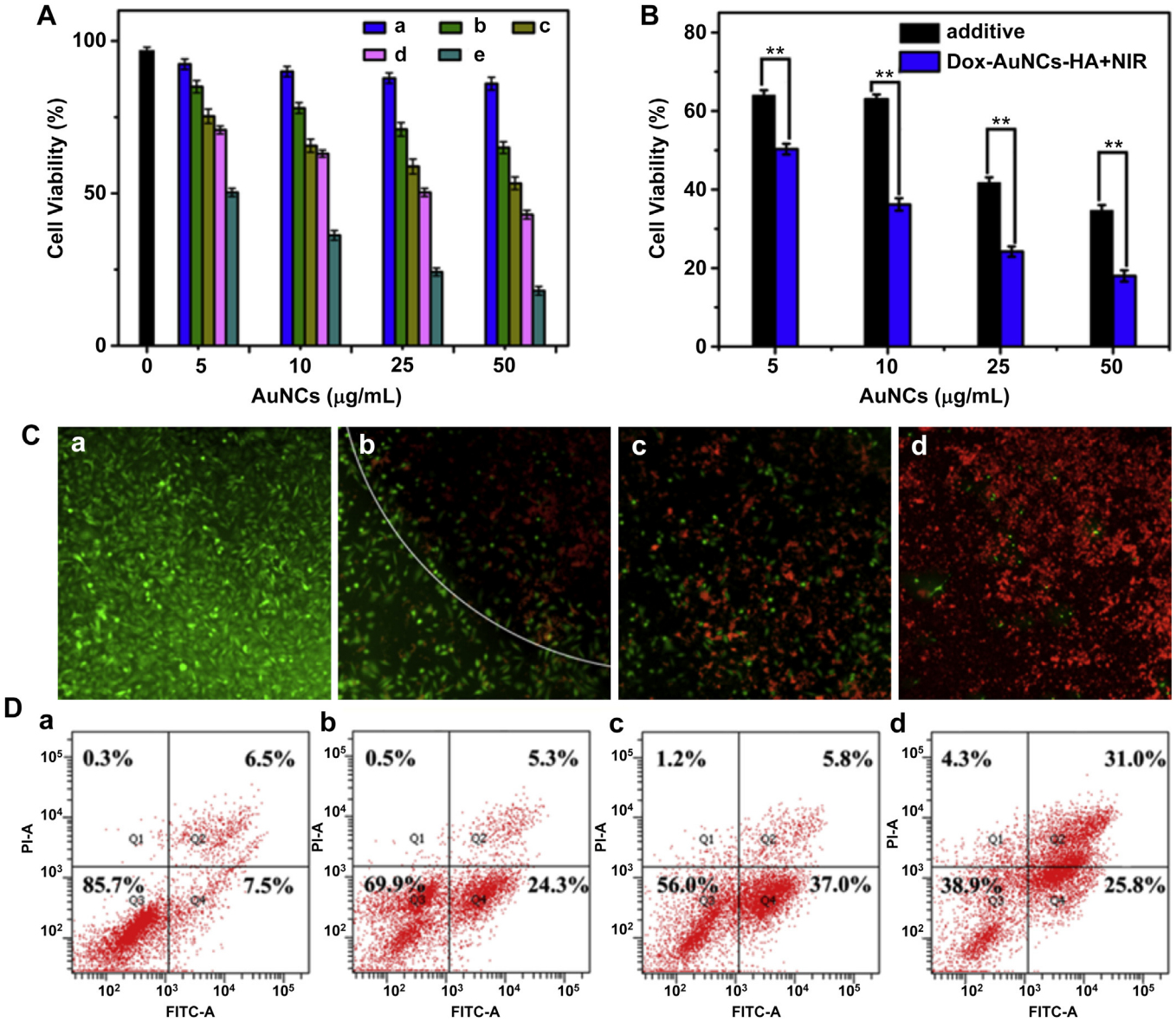

Fig. 7. A) Viability of MDA-MB-231 cells incubated for 24 h with different concentrations of nanoparticles. (a) AuNCs-HA, (b) AuNCs-HA upon NIR irradiation (0.5 h, 43 °C) (c) Dox-AuNCs-HA, (d) free Dox, (e) Dox-AuNC-HA upon NIR irradiation (0.5 h, 43 °C). B) The efficacy of synergistic treatment is compared with the additive efficacy of independent photothermal therapy and chemotherapy using *t*-tests with all *p*-values lower than 0.01. Asterisks indicate statistically significant differences ($^{*}P < 0.05$, $^{**}P < 0.01$, $^{***}P < 0.001$). C) Fluorescence microscopy images of MDA-MB-231 cells incubated with AuNCs-HA (a), AuNCs-HA upon 808 nm NIR irradiation (b), Dox-AuNCs-HA (c), Dox-AuNCs-HA upon 808 nm NIR irradiation (d). Viable cells were stained green with calcein AM, dead cells were stained red with PI. All images were obtained under magnification of 10. D) Flow cytogram representing apoptosis assay based on Annexin V-FITC and PI staining of MDA-MB-231 cells. (a) Control cells, (b) AuNCs-HA upon NIR irradiation (0.5 h, 43°C), (c) Dox-AuNCs-HA, (d) Dox-AuNCs-HA upon NIR irradiation (0.5 h, 43 °C). (For interpretation of the references to colour in this figure legend, the reader is referred to the web version of this article.)

likely that AuNCs-HA accumulated in the tumor sites via receptor–ligand interaction between HA and CD44 over-expressing cells [51]. However, the most of Au amount were accumulated in liver in both cases of AuNCs and AuNCs-HA, which owing to the strong phagocytosis in reticuloendothelial system (RES) organs [52,53]. For other organs, there were no significant difference between the uptake of AuNCs and AuNCs-HA. Considering the above results, we next investigated the efficacy in regressing tumor growth of our system by directed intratumoral injection. After the tumor size reached about 200 mm^3, the drug efficacy was studied in four groups of MDA-MB-231 tumor-bearing mice ($n = 5$ per group), with tumor size differences minimized among the groups. Therefore, the results of 5 mice in each group could accurately and comprehensively assess the in vivo antitumor efficacy. Four regimens were administered by a single intratumoral injection, with a dose of 0.1 mg/mL nanocomposites per mouse in MDA-MB-231 tumor model. As shown in Fig. 8B, the mice treated only with 0.9% NaCl solution exhibited a rapid increasing in tumor size. Subsequently, we studied the photothermal property of AuNCs in vivo. An IR thermal camera was used to monitor the temperatures changes on mice. Upon NIR irradiation (1 W/cm^2, 5 min), mice treated with AuNCs-HA showed localized heating in the tumor regions (Fig. 8C) and the relative tumor size was slightly reduced compared to control group (Fig. 8B). For treatment with Dox-AuNCs-HA alone, enhanced inhibition of tumor growth was observed. Unfortunately, the solid tumors could not been eliminated completely. By treating the solid tumors with Dox-AuNCs-HA and NIR irradiation together, we could found that all the tumors were eliminated completely

Please cite this article in press as: Wang Z, et al., A multi-stimuli responsive gold nanocage–hyaluronic platform for targeted photothermal and chemotherapy, Biomaterials (2014), http://dx.doi.org/10.1016/j.biomaterials.2014.08.013

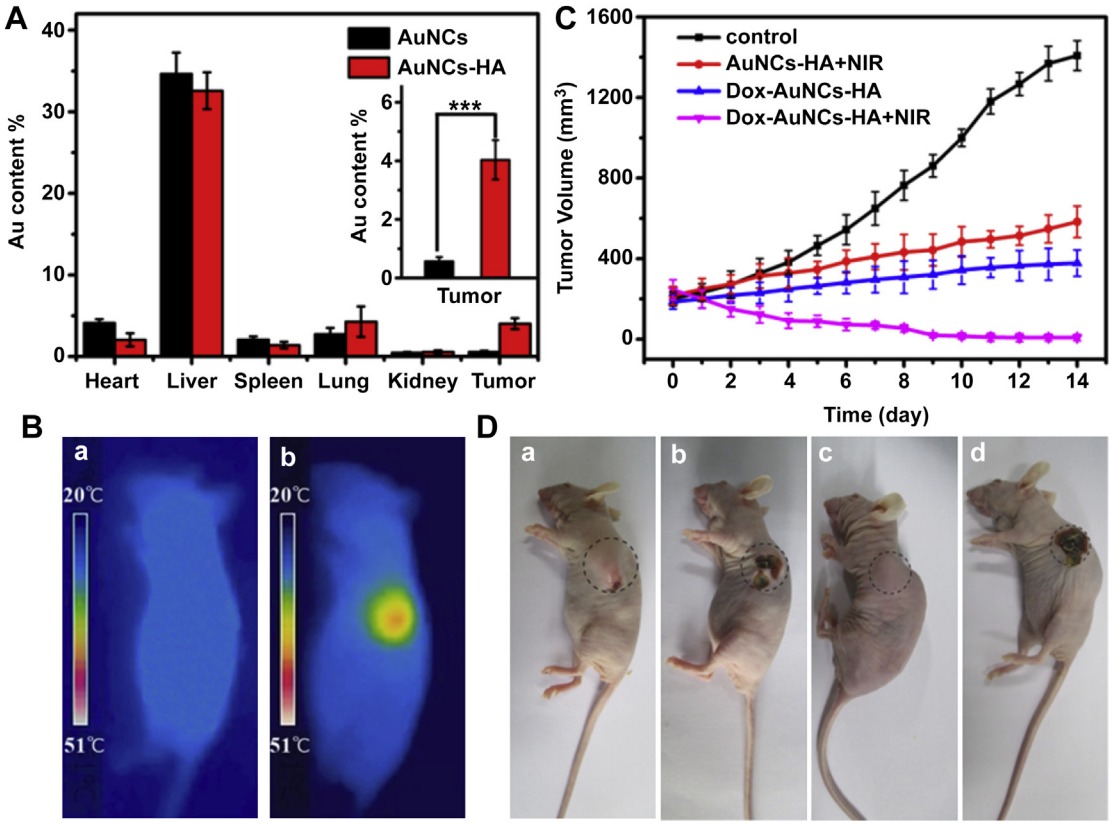

Fig. 8. A) Biodistribution of AuNCs and AuNCs-HA in main organs at 24 h post-injection ($n = 3$). Gold concentrations were analyzed by ICP-MS. Asterisks indicate statistically significant differences ($^{*}P < 0.05$, $^{**}P < 0.01$, $^{***}P < 0.001$). B) In vivo photothermal tumor heating. IR thermal images of tumor-bearing mice treated with 50 μL AuNCs-HA without NIR laser (a) and with NIR laser (1 W/cm^2, 5 min, b). C) The relative tumor volumes of nude mice ($n = 5$) treated with 0.9% NaCl solution (control), AuNCs-HA nanoparticles upon NIR irradiation, Dox-AuNCs-HA nanoparticles, and Dox-AuNCs-HA nanoparticles upon NIR irradiation. D) The picture of tumors after different treatments at 14d, (a) control, (b) AuNCs-HA upon NIR irradiation, (c) Dox-AuNCs-HA, (d) Dox-AuNCs-HA upon NIR irradiation. (For interpretation of the references to colour in this figure legend, the reader is referred to the web version of this article.)

within 9 days, indicating the excellent synergistic effect of combining photothermal therapy and chemotherapy. Otherwise, visible tumor sizes upon different treatments were provided in Fig. 8D. Taken together, we further confirmed our design that the Dox-AuNCs-HA nanoparticles could utilized as efficient antitumor agents.

4. Conclusion

In summary, we have successfully demonstrated a multifunctional platform that coupled multiple modalities: targeting, multi-stimuli responsive and pinpointed intracellular drug release, as well as chemo-photothermal synergistic therapy for solid tumors. Our multi-stimuli responsive system only released Dox from Dox-AuNCs-HA in intracellular environments, such as endosomal and lysosomal vesicles, where HA was degraded by intracellular Hyal. Our system acted as a high-performance nanocarrier and ensured that only internalized nanocomposites could response to the multi-stimuli. Beyond that, NIR light irradiation further enhanced the release of Dox from Dox-AuNCs-HA in cancer cells and dramatically improved the therapeutic efficacy. Both in vitro and in vivo results demonstrated that the combination of photothermal therapy and chemotherapy resulted in harsh cell toxicity, while chemotherapy or photothermal treatment alone could not achieve these outcomes. In light of these advantages, our work may promote the design of noninvasive and pinpointed drug release systems to minimize non-specific systemic spread of toxic drugs and to maximize tumor-directed drug delivery efficiency.

Acknowledgments

The authors are grateful for the referee's helpful comments on the manuscript. Financial support was provided by the National Basic Research Program of China (2012CB720602 and 2011CB936004) and the National Natural Science Foundation of China (Grants 91213302, 21210002 and 21431007).

Appendix A. Supplementary data

Supplementary data related to this article can http://dx.doi.org/10.1016/j.biomaterials.2014.08.013.

References

[1] Klaikherd A, Nagamani C, Thayumanavan S. Multi-stimuli sensitive amphiphilic block copolymer assemblies. J Am Chem Soc 2009;131:4830–8.
[2] Wang K, Guo DS, Wang X, Liu Y. Multistimuli responsive supramolecular vesicles based on the recognition of p-sulfonatocalixarene and its controllable Release of doxorubicin. ACS Nano 2011;5:2880–94.
[3] Zhu YF, Shi JL, Shen WH, Dong XP, Feng JW, Ruan ML, et al. Stimuli-responsive controlled drug release from a hollow mesoporous silica sphere/polyelectrolyte multilayer core-shell structure. Angew Chem 2005;117:5213–7.
[4] Chen CE, Pu F, Huang ZZ, Liu Z, Ren JS, Qu XG. Stimuli-responsive controlled-release system using quadruplex DNA-capped silica nanocontainers. Nucleic Acids Res 2011;39:1638–44.
[5] Cheng R, Meng FH, Deng C, Klok HA, Zhong ZY. Dual and multi-stimuli responsive polymeric nanoparticles for programmed site-specific drug delivery. Biomaterials 2013;34:3647–57.
[6] Liu JN, Bu WB, Pan LM, Shi JL. NIR-triggered anticancer drug delivery by upconverting nanoparticles with integrated azobenzene-modified mesoporous Silica. Angew Chem Int Ed 2013;52:4375–9.

[7] Wu SS, Huang X, Du XZ. Glucose- and pH-responsive controlled release of cargo from protein-gated carbohydrate-functionalized mesoporous silica nanocontainers. Angew Chem Int Ed 2013;52:5580–4.
[8] Wei J, Ju XJ, Zou XY, Xie R, Wang W, Liu LY, et al. Multi-stimuli-responsive microcapsules for adjustable controlled-release. Adv Funct Mater 2014;24:3312–23.
[9] Bae Y, Fukushima S, Harada A, Kataoka. Design of environment-sensitive supramolecular assemblies for intracellular drug delivery: polymeric micelles that are responsive to intracellular pH change. Angew Chem Int Ed 2003;42:4640–3.
[10] Abidian MR, Kim DH, Martin DC. Conducting-polymer nanotubes for controlled drug release. Adv Mater 2006;18:405–9.
[11] Wang Y, Wang KY, Zhao JF, Liu XG, Bu J, Yan XY. Multifunctional mesoporous silica-coated graphene nanosheet used for chemo-photothermal synergistic targeted therapy of glioma. J Am Chem Soc 2013;135:4799–804.
[12] Chen CE, Geng J, Pu F, Yang XJ, Ren JS, Qu XG. Polyvalent nucleic acid/mesoporoussilica nanoparticle conjugates:dual stimuli-responsive vehicles for intracellular drug delivery. Angew Chem Int Ed 2010;50:882–6.
[13] Chen HB, Xiao L, Anraku Y, Mi P, Liu XY, Cabral H, et al. Polyion complex vesicles for photo-induced intracellular delivery of amphiphilic photosensitizer. J Am Chem Soc 2014;136:157–63.
[14] Lai CY, Trewyn BG, Jeftinija DM, Jeftinija K, Xu S, Jeftinija S, et al. A mesoporous silica nanosphere-based carrier system with chemically removable CdS nanoparticle caps for stimuli-responsive controlled release of neurotransmitters and drug molecules. J Am Chem Soc 2003;125:4451–9.
[15] Dai J, Lin SD, Cheng D, Zou S, Shuai XT. Interlayer-crosslinked micelle with partially hydrated core showing reduction and pH dual sensitivity for pinpointed intracellular drug release. Angew Chem Int Ed 2011;50:9404–8.
[16] Fattahi P, Borhan A, Abidian MR. Microcapsulation of chemotherapeutics into monodisperse and tunable biodegradable polymers via electrified liquid jets: control of size, shape, and drug release. Adv Mater 2013;25:4555–60.
[17] He QJ, Gao Y, Zhang LX, Zhang ZW, Gao F, Ji XF, et al. A pH-responsive mesoporous silica nanoparticles-based multi-drug delivery system for overcoming multi-drug resistance. Biomaterials 2011;32:7711–20.
[18] Lee JH, Chen KJ, Noh SH, Garcia MA, Wang H, Lin WY, et al. On-demand drug release system for in vivo cancer treatment through self-assembled magnetic nanoparticles. Angew Chem Int Ed 2013;52:4384–8.
[19] Tian JW, Ding L, Xu HJ, Shen Z, Ju HX, Jia L. Cell-specific and pH-activatable rubyrin-loaded nanoparticles for highly selective near-infrared photodynamic therapy against cancer. J Am Chem Soc 2013;135:18850–8.
[20] Chen JY, Glaus C, Laforest R, Zhang Q, Yang MX, Gidding M, et al. Gold nanocages as photothermal transducers for cancer treatment. Small 2010;6:811–7.
[21] Moon GD, Choi SW, Cai X, Li WY, Cho EC, Jeong U, et al. A new theranostic system based on gold nanocages and phase-change materials with unique features for photoacoustic imaging and controlled release. J Am Chem Soc 2011;133:4762–5.
[22] Chen JY, Saeki F, Wiley BJ, Cang H, Cobb MJ, Li ZY, et al. Gold nanocages: bioconjugation and their potential use as optical imaging contrast agents. Nano Lett 2005;5:473–7.
[23] Zhou J, Lu ZG, Zhu XJ, Wang XJ, Liao Y, Ma ZY, et al. NIR photothermal therapy using polyaniline nanoparticles. Biomaterials 2013;34:9584–92.
[24] Li N, Yu ZZ, Pan W, Han YY, Zhang TY, Tang B. A near-infrared light-triggered nanocarrier with reversible DNA valves for intracellular controlled release. Adv Funct Mater 2013;23:2255–62.
[25] Yagüe C, Arruebo M, Santamaria J. NIR-enhanced drug release from porous Au/SiO2 nanoparticles. Chem Commun 2010;46:7513–5.
[26] Yang XJ, Liu X, Liu Z, Pu F, Ren JS, Qu XG. Near-infrared light-triggered, targeted drug delivery to cancer cells by aptamer gated nanovehicles. Adv Mater 2012;24:2890–5.
[27] Yang JP, Shen DK, Zhou L, Li W, Li XM, Yao C, et al. Spatially confined fabrication of core-shell gold nanocages@mesoporous silica for near-infrared controlled photothermal drug release. Chem Mater 2013;25:3030–7.
[28] Hong S, Yang K, Kang B, Lee CY, Song IT, Byun EY, et al. Hyaluronic acid catechol: a biopolymer exhibiting a pH-dependent adhesive or cohesive property for human neural stem cell engineering. Adv Funct Mater 2013;23:1774–80.
[29] Lee BY, Lee H, Kim YB, Kim J, Hyeon T, Park HW, et al. Bioinspired surface immobilization of hyaluronic acid on monodisperse magnetite nanocrystals for targeted cancer imaging. Adv Mater 2008;20:4154–8.
[30] Luo Y, Ziebell MR, Prestwich GD. A hyaluronic acid-taxol antitumor bioconjugate targeted to cancer cells. Biomacromolecules 2000;1:208–18.
[31] Zhang F, Wan Y, Yu T, Zhang F, Shi Y, Xie S, et al. Uniform nanostructured arrays of sodium rare-earth fluorides for highly efficient multicolor upconversion luminescence. Angew Chem Int Ed 2007;46:7976–9.
[32] Choi KY, Chung HJ, Min KH, Yoon HY, Kim K, Park, et al. Self-assembled hyaluronic acid nanoparticles for active tumor targeting. Biomaterials 2010;31:106–14.
[33] Li LH, Qian Y, Jiang C, Lv YG, Liu WQ, Zhong L, et al. The use of hyaluronan to regulate protein adsorption and cell in filtration in nanofibrous scaffolds. Biomaterials 2012;33:3428–45.
[34] Luo Y, Bernshaw NJ, Lu ZR, Kopecek J, Prestwich GD. Targeted delivery of doxorubicin by HPMA copolymer-hyaluronan bioconjugates. Pharm Res 2002;19:396–402.
[35] Yoon HY, Koo H, Choi KY, Lee SJ, Kim K, Kwon IC, et al. Tumor-targeting hyaluronic acid nanoparticles for photodynamic imaging and therapy. Biomaterials 2012;33:3980–9.
[36] Bhang SH, Won N, Lee TJ, Jin H, Nam J, Park J, et al. Hyaluronic acidquantum dot conjugates for in vivo lymphatic vessel imaging. ACS Nano 2009;3:1389–98.
[37] Choi KY, Yoon HY, Kim JH, Bae SM, Park RW, Kang YM, et al. Smart nanocarrier based on PEGlated hyaluronic acid for cancer therapy. ACS Nano 2011;5:8591–9.
[38] Kamat M, El-Boubbou, Zhu DC, Lansdell T, Lu XW, Li W, et al. Hyaluronic acid immobilized magnetic nanoparticles for active targeting and imaging of macrophages. Bioconjugate Chem 2010;21:2128–35.
[39] Li J, Huo MR, Wang J, Zhou JP, Mohammad MJ, Zhang YL, et al. Redox-sensitive micelles self-assembled from amphiphilic hyaluronic acid-deoxycholic acid conjugates for targeted intracellular delivery of paclitaxel. Biomaterials 2012;33:2310–20.
[40] Ma M, Chen HR, Chen Y, Zhang K, Wang X, Cui XZ, et al. Hyaluronic acid-conjugated mesoporous silica nanoparticles: excellent colloidal dispersity in physiological fluids and targeting efficacy. J Mater Chem 2012;22:5615–21.
[41] Sherlock SP, Tabakman SM, Xie LM, Dai HJ. Photothermally enhanced drug delivery by ultrasmall multifunctional FeCo/graphitic shell nanocrystals. ACS Nano 2011;5:1505–12.
[42] Shi P, Li M, Ren JS, Qu XG. Gold nanocage-based dual responsive “caged metal chelator” release system: noninvasive remote control with near infrared for potential treatment of alzheimer's disease. Adv Funct Mater 2013;23:5412–7.
[43] Min H, Cowman MK. Combined alcian blue and silver staining of glycosaminoglycans in polyacrylamide gels: application to electrophoretic analysis of molecular weight distribution. Anal Biochem 1986;155:275–85.
[44] Bhirde AA, Kapoor A, Liu G, Iglesias-Bartolome R, Jin A, Zhang G, et al. Nuclear mapping of nanodrug delivery systems in dynamic cellular environments. ACS Nano 2012;6:4966–72.
[45] Gong H, Cheng L, Xiang J, Xu H, Feng LZ, Shi XZ, et al. Near-infrared absorbing polymerics as a versatile drug carrier for cancer combination therapy. Adv Funct Mater 2013;23:6059–67.
[46] Swierczewska M, Choi KY, Mertz EL, Huang X, Zhang F, Zhu L, et al. A facile, one-step nanocarbon functionalization for biomedical applications. Nano Lett 2012;12:3613–20.
[47] Wang F, Wang YC, Dou S, Xiong MH, Sun TM, Wang J. Doxorubicin-tethered responsive gold nanoparticles facilitate intracellular drug delivery for overcoming multidrug resistance in cancer Cells. ACS Nano 2011;5:3679–92.
[48] Zhang ZJ, Wang J, Nie X, Wen T, Ji YL, Wu XC, et al. Near infrared laser induced targeted cancer therapy using thermoresponsive polymer encapsulated gold nanorods. J Am Chem Soc 2014;136:7317–26.
[49] Rim HP, Min KH, Lee HJ, Jeong SY, Lee SC. pH-tunable calcuim phosphate covered mesoporous silica nanocontainers for intrcellular controlled release of guest drugs. Angew Chem Int Ed 2011;50:8853–7.
[50] Hauck TS, Jennings TL, Yatsenko T, Kumaradas JC, Chan WCW. Enhancing the toxicity of cancer chemotherapeutics with gold nanorod hyperthermia. Adv Mater 2008;20:3832–8.
[51] Lim EK, Kim HO, Jang E, Park J, Lee K, Suh JS, et al. Hyaluronan-modified magnetic nanoclusters for detection of CD44-overexpressing breast cancer by MR imaging. Biomaterials 2011;32:7941–50.
[52] Guo LR, Yan DD, Yang DF, Li YJ, Wang XD, Zalewski O, et al. Combinatorial photothermal and immuno cancer therapy using chitosan-coated hollow copper sulfide nanoparticles. ACS Nano 2014. http://dx.doi.org/10.1021/nn5002112.
[53] Qhattal HSS, Hye T, Alali A, Liu XL. Hyaluronan polymer length, grafting density, and surface poly (ethylene glycoal) coating influence in vivo circulation and tumor targeting of hyaluronan-grafted liposomes. ACS Nano 2014. http://dx.doi.org/10.1021/nn405839n.

Please cite this article in press as: Wang Z, et al., A multi-stimuli responsive gold nanocage–hyaluronic platform for targeted photothermal and chemotherapy, Biomaterials (2014), http://dx.doi.org/10.1016/j.biomaterials.2014.08.013